Proc. Natl. Acad. Sci. USA
Vol. 93, pp. 5341–5346, May 1996
Cell Biology

Direct observation of iron-induced conformational changes of mitochondrial DNA by high-resolution field-emission in-lens scanning electron microscopy

(DNA unwinding/iron colloid formation/backscattered electron detection)

MARCUS YAFFEE*†‡, PATRICK WALTER†, CHRISTOPH RICHTER†, AND MARTIN MÜLLER*

*Laboratory for Electron Microscopy I and †Laboratory for Biochemistry I, Swiss Federal Institute of Technology (ETH), CH-8092 Zürich, Switzerland

Communicated by K. Wüthrich, Eidgenössische Technische Hochschule, Zurich, Switzerland. January 24, 1996 (received for review June 21, 1995)

ABSTRACT **When respiring rat liver mitochondria are incubated in the presence of Fe(III) gluconate, their DNA (mtDNA) relaxes from the supercoiled to the open circular form dependent on the iron dose. Anaerobiosis or antioxidants fail to completely inhibit the unwinding. High-resolution field-emission in-lens scanning electron microscopy imaging, in concert with backscattered electron detection, pinpoints nanometer-range iron colloids bound to mtDNA isolated from iron-exposed mitochondria. High-resolution field-emission in-lens scanning electron microscopy with backscattered electron detection imaging permits simultaneous detailed visual analysis of DNA topology, iron dose-dependent mtDNA unwinding, and assessment of iron colloid formation on mtDNA strands.**

Mitochondria accumulate iron in the form of Fe(III) (1–3) and then can reduce it to Fe(II) (4). Mitochondrial iron is necessary for incorporation into iron–sulfur proteins and heme (5) but is potentially dangerous because it participates in hydroxyl radical (·OH) formation (6). Mitochondria are the major source of superoxide (7), which can dismutate to yield hydrogen peroxide. This, in turn, can interact with Fe(II) to produce ·OH radicals. They can damage DNA in many ways, particularly by inducing single-strand breaks (SSB) (8), which leads to changes in mtDNA conformation (9–13).

Mammalian mtDNA possesses three archetypal conformations: form I, supercoiled; form II, open relaxed; and form III, linear. Form I is believed to predominate *in vivo*.§ mtDNA is a compact molecule coding for 2 rRNAs, 22 tRNAs, and 13 peptides [rat mtDNA has 16,298 bp (16)]. This leaves mtDNA with few noncoding regions; damage to the mtDNA could therefore be metabolically devastating. Indeed, modifications of mtDNA—*e.g.*, point mutations, fragmentation, deletions, and duplications—have been etiologically linked to human diseases (17) and to aging (18). Since oxidative damage to mtDNA is 16-fold greater than that to nuclear DNA (19), oxidative stress could contribute significantly to disease-related mtDNA modifications (20).

Here we establish a method for high-resolution field-emission in-lens scanning electron microscopy (HR-SEM) observation of the three-dimensional structure of native DNA topology. We thereby detect an iron-induced shift of mtDNA from the supercoiled to the open circular forms. HR-SEM analysis with backscattered electron (BSE) detection also allowed us to localize and identify colloidal iron species on mtDNA. Because the exact structure and composition of these aggregates are not yet known, we refer to them as colloids. Colloids are microheterogeneous structures with dimensions in the range from 1 to 1000 nm (21, 22).

The publication costs of this article were defrayed in part by page charge payment. This article must therefore be hereby marked "*advertisement*" in accordance with 18 U.S.C. §1734 solely to indicate this fact.

MATERIALS AND METHODS

mtDNA Preparation. Female Wistar rat liver mitochondria were isolated by differential centrifugation (23) and incubated with up to 500 μM Fe(III) gluconate for 20 min, with stirring, in an oxygen-saturated buffer, consisting of 10 mM *N*-(2-hydroxyethyl)piperazine-*N'*-(2-ethanesulfonic acid) (Hepes), 5 mM $MgCl_2$, 10 mM KCl, 225 mM sucrose, pH 7.4, with 2.5 mM succinate as substrate. Fe(III) gluconate complexes were synthesized by oxidative hydrolysis (2), which yields Fe(III) gluconate that is characterized as to structure (24, 25) and bioavailability (2, 3). Nitrogen (99.995%)-purged solutions of 20 mM potassium D-gluconate and 100 mM Hepes (pH 7.4) were made, to which an equal volume of 20 mM nitrogen-purged $FeCl_2$ was added. This Fe(II) solution was completely oxidized by purging with 100% oxygen for 30 min. Chelation of the 1:1 Fe(III):gluconate complexes by succinate was ruled out by speciation calculations as follows: even though the acid dissociation constants of gluconate and succinate are similar (26), there is no Fe(III) succinate species at pH 7.4 when the Fe(III):gluconate molar ratio is 1:1, due to structural differences between gluconate and succinate. At low pH the carboxylates are the sole donors to Fe(III), but at pH 7.4 the hydroxyl groups of gluconate become deprotonated with assistance of the strong Lewis acid Fe(III). The gluconate becomes tetradentate in turn. Its capacity to chelate then exceeds that of succinate, which is only bidentate. The logarithm of the stability constant of the 3-fold deprotonated Fe(III) gluconate complex is calculated from Martell and Motekaitis (26) as 35.6. Analogously, the logarithm of the stability constant of the Fe(III) succinate complex is only 6.9. Because both species are of the same stochiometry, the data can be compared directly. Thus, at equimolar or excessive Fe(III):gluconate ratio, the Fe(III) gluconate complex is the only significant Fe(III) species. Fe(III) gluconate uptake (2, 3) by respiring mitochondria was confirmed by using ^{59}Fe [Amersham; 0.143 mCi/mg of Fe(III); 1 Ci = 37 GBq] -labeled Fe(III) gluconate complexes in combination with Millipore filtration as described for $^{45}Ca^{2+}$ transport (27).

In anaerobic experiments the extent of oxygen depletion by nitrogen purging and glucose oxidase [EC 1.1.3.4, $K_m = 2.0 \times 10^{-4}$ M (28); Fluka] addition was monitored by a Clark electrode (Yellow Springs Instruments). The oxygen concentration was below 0.5 μM, as determined by dithionite and glucose oxidase calibration of the oxygen electrode.

Abbreviations: BSE, backscattered electron; DARS, double-axis rotary shadowing; HR-SEM, high-resolution field-emission in-lens scanning electron microscopy; SE, secondary electron; SSB, single-strand breaks.

‡To whom reprint requests should be addressed at: Biochemistry I, CHN-N33, Swiss Federal Institute of Technology, CH-8092 Zürich Switzerland.

§HR-SEM identification of form I mtDNA, combined with electrophoresis data of isolated mtDNA, strongly suggest that a specific level of supercoiling is present *in vivo*. The existence of mitochondrial topoisomerases supports this hypothesis (14, 15).

mtDNA was isolated by neutral lysis of mitochondria in 1.5% SDS, precipitation of membranes and proteins by 5 M NaCl, followed by two phenol/chloroform (1:1) and chloroform extractions, ethanol precipitation and centrifugation. The resulting mtDNA pellet was washed with 80% ethanol and resuspended, then further purified on a Sephacryl S-400 mini-spun column. Samples were electrophoresed at constant current, 67 mA (4 V/cm) for 90 min on a 0.7% agarose gel with 0.5 μg/ml ethidium bromide. The gel was photographed under UV illumination, and the negative was scanned on a Molecular Dynamics laser densitometer. Error shown is standard error of the mean.

Sample Preparation and HR-SEM Observation. pBR322, pUC21, and mtDNA samples were dialyzed against 3 mM $MgCl_2$ by centrifugation/filtration in Centricon-30 concentrators (3 × 30 min at 5000× *g*) (Amicon). DNA was adjusted to ~300 ng/ml and placed in 20-μl droplets on parafilm (29). Carbon/collodion-coated 400-mesh copper grids, freshly etched by a charged oxygen plasma [30 sec, 100 mV, 5 mbar of O_2 (1 mbar = 100 Pa) in a Balzers GEA-003-S glow-discharge apparatus (Balzers), were placed on the droplets for 2 min, removed perpendicularly to the surface, immediately plunge-frozen in liquid nitrogen, and transferred under liquid nitrogen to the stage of a precooled (−160°C) Balzers BAF-300 freeze-etch machine. Samples were kept at 2×10^{-7} mbar and −100°C for 2 hr, and then double-axis rotary-shadowed (30) with chromium metal (≈1 nm thick). They were then brought to 20°C under vacuum and removed from the BAF-300.

Samples were next placed in a Hitachi S-900 field-emission in-lens HR-SEM on a Gatan cryoholder, and brought to −85°C to reduce contamination (30). This S-900 is equipped with a highly sensitive yttrium/aluminum garnet single-crystal BSE detector (31). Primary magnifications ranged from ×50,000 to ×400,000. Astigmatism was corrected to ×800,000 on chromium metal grains. Fine focusing was done during the first lines of the photoscan. Images of DNA surface topology were generated by the secondary electron (SE) signal; the material-dependent BSE images were used to localize the metal colloids. BSE and SE signals were recorded in parallel on film; they were also digitally acquired simultaneously using Gatan Digiscan equipment and Digital Micrograph software (Gatan, Pleasanton, CA). Negatives were scanned and digitized (Leafscan Model 45 film scanner, Leaf Systems, Southborough, MA). DNA length was calculated from digitized images (DIGITAL MICROGRAPH 2.1B, Gatan) and from micrographs processed with a Bit Pad Plus (model CR 1212, Summagraphics, Fairfield, CT). For quanitation of mtDNA forms in HR-SEM, all micrographs were pooled and the proportion of each form was calculated.

HR-SEM of Colloids. Experiments to verify the presence of iron in the colloids were performed as follows: (*i*) Fe(III) gluconate solutions were plunge-frozen and analyzed with HR-SEM SE/BSE imaging for metal colloids. (*ii*) Incubation solutions with or without (see Fig. 4 *e* and *f*) DTPA (20 mM) were treated analogously. (*iii*) mtDNA isolated from mitochondria incubated with or without iron, and mtDNA treated with or without DTPA after isolation, was also analyzed by cryo-HR-SEM. (*iv*) Two iron colloids, 30 and 100 nm in diameter (a gift of Felix Funk, Institute of Terrestrial Ecology, Eidgenössische Technische Hochschule, Zürich), were imaged in BSE and SE modes for reference (see Fig. 4 *a* and *b insets*). (*v*) Isolated mtDNA was mixed with either Fe(III) gluconate, or Fe(III) gluconate plus incubation solution, or the iron reference colloids (described above), and analyzed with cryo-HR-SEM.

RESULTS

Conformational Analysis. DNA plasmids pBR322 and pUC21 were chosen as HR-SEM specimen controls because of their known sequences (32, 33) and conformational similarity to mtDNA. HR-SEM micrographs of plasmids and mtDNA display individual variations within the categories of DNA topology defined through gel electrophoresis (Figs. 1 and 2). pUC21 (Fig. 1*a*) and untreated mtDNA (Fig. 1*b*) exhibit extensive supercoiling. Fig. 2*a* shows a partially unwound pUC21 plasmid with two tightly supercoiled regions (primary magnification ×350,000). Fig. 2*b* displays a higher magnification of a double stranded-region of the same plasmid. Measurements of open circular pUC21 DNA (3200 bp, open-circular pUC21 not shown), pBR322 DNA (4361 bp, Fig. 2 *c* and *d*), and mtDNA (16,298 bp, Fig. 2*e*) gave lengths of 1090 ± 5 nm ($n = 18$, n is the number of molecules measured), 1483 ± 5 nm ($n = 16$), and 5540 nm ± 16 nm, ($n = 14$), respectively. These values are consistent with the 0.34 nm rise between base pairs (34, 35). The length of mtDNA estimated by our gel electrophoresis is about 16,300 bp, which agrees with the above HR-SEM data and previous sequence data (16). This establishes pUC21 and pBR322 as reliable standards for conformational studies of mtDNA. Open-circular mtDNA displays well-defined displacement-loop structures (Fig. 2*e*, arrow). The average size of the displacement loops is 205.1 nm ± 24.6 nm or 603 bp ($n = 16$). The width of the double-stranded DNA is 2.7 ± 0.2 nm ($n = 92$), close to the expected value of 2 nm for DNA, considering that there is less than 1 nm of chromium coating (30, 36).

HR-SEM SE images (Figs. 2*e* and 4 *a*, *c*, and *e*) document that mtDNA relaxes to the open-circular form in a dose-dependent manner when Fe(III) gluconate is taken up by mitochondria *in vitro*. Fig. 4 *c* and *d* reveal colloids bound between two duplex mtDNA strands.

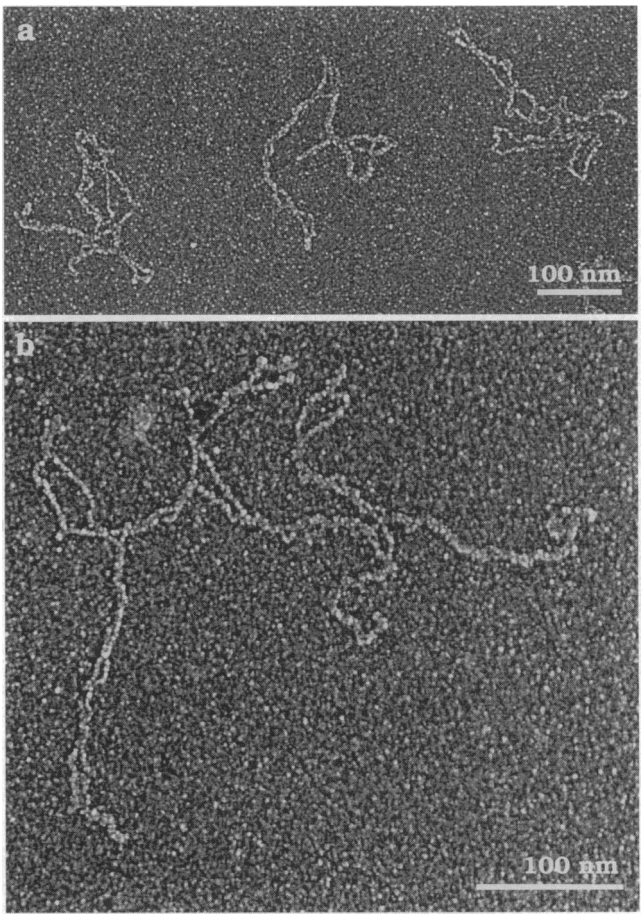

FIG. 1. HR-SEM imaging of three-dimensional surface topology of supercoiled plasmids of pUC21 (*a*) and DNA obtained from control mitochondria (*b*). Plasmid and mitochondrial DNA were prepared as described in the text. HR-SEM imaging permits direct observation of tight twisting in the supercoils of DNA.

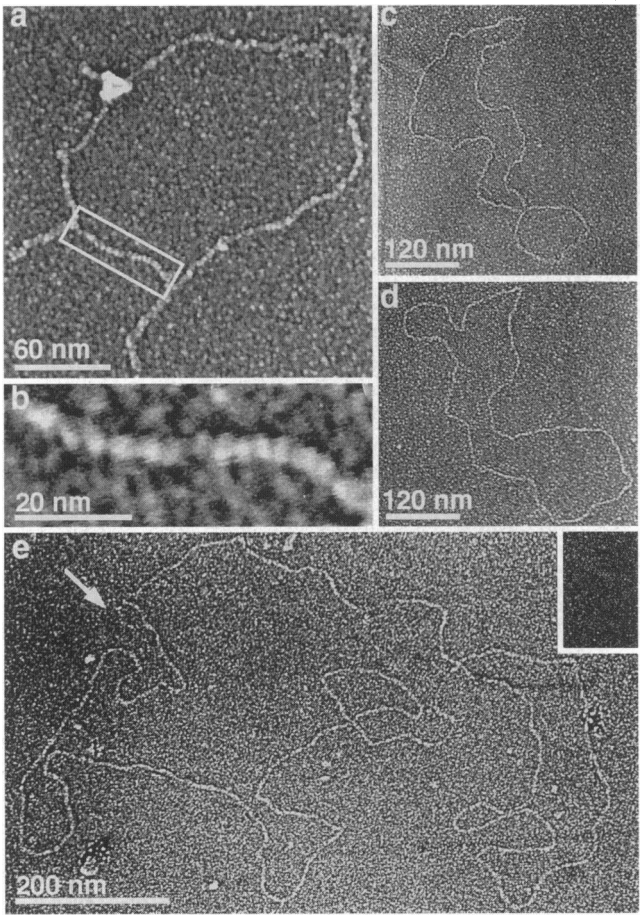

FIG. 2. Open-circular DNA molecules. (*a*) Overview of pUC21 DNA (×350,000 primary magnification); (*b*) higher magnification of a selected area of pUC21 DNA; (*c* and *d*) pBR322 DNA; (*e*) mtDNA isolated from mitochondria incubated with 500 μM Fe(III) gluconate. During the isolation of this mtDNA sample, the metal chelator, DTPA, was present in the resuspension and lysis buffers; backscattered image (*inset*) displays the absence of iron colloids. The arrow shows a displacement loop of 102 nm (300 bp).

Gel electrophoresis substantiates the HR-SEM findings (Fig. 3). Densitometric analysis establishes the relative levels of open-circular mtDNA and SSB (Fig. 3 *b* and *c*). The two methods yield similar results. Thus, control mtDNA (isolated from unexposed, incubated mitochondria) shows 64.5 ± 2.8% form I and 34.8 ± 3% form II (n = 14; n is the number of mitochondrial isolations) upon electrophoresis, whereas HR-SEM displays 77% form I and 23% form II (n = 76, n is the number of molecules analyzed[¶]). The level of form III is negligible and remains unchanged. The fraction of form II increases with larger doses of Fe(III) gluconate: When mitochondria are incubated with 500 μM Fe(III) gluconate, electrophoresis shows 74.5 ± 6% form II and 25.2 ± 6% form I mtDNA (n = 14, Fig. 3*b*), whereas HR-SEM reveals 80% form II and 20% form I (n = 11). SSB [SSB/mtDNA molecule, calculated from the equation SSB = $-\ln(1.4 \times \text{form I})/(1.4 \times \text{form I} + \text{form II})$][‖] increase concomitantly with increasing doses of Fe(III) gluconate. Incubation of mitochondria with 500 μM Fe(III) gluconate at oxygen concentrations below 0.5 μM resulted in a 43.3 ± 2% (n = 3; n is the number of mitochondrial isolations) reduction in the amount of SSB (relative to the amount of SSB under normoxic conditions). When mitochondria were incubated under normoxic conditions, the presence of the antioxidants butylated hydroxytolu-

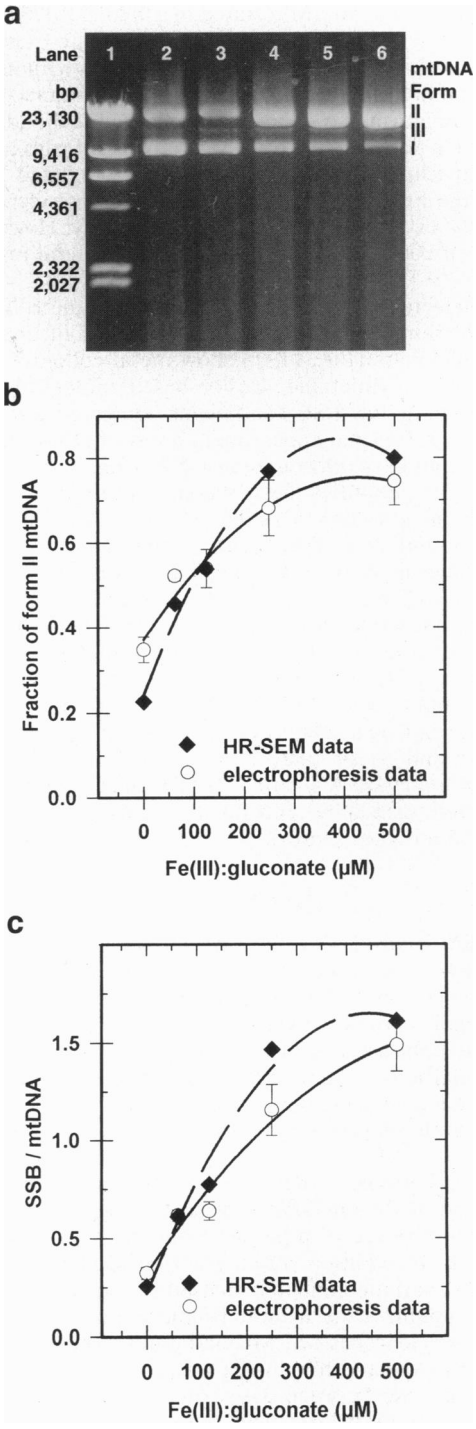

FIG. 3. Gel electrophoresis, densitometry and quantification of mtDNA isolated from mitochondria exposed to Fe(III) gluconate. (*a*) Gel electrophoresis: Lane 1, bacteriophage λ DNA cleaved with *Hin*dIII; lane 2, control mtDNA isolated directly from mitochondria; lane 3, control mtDNA isolated from mitochondria incubated without iron; lanes 4–6, mtDNA isolated from mitochondria incubated with 63, 250, and 500 μM Fe(III) gluconate, respectively. (*b* and *c*) Densitometric analysis: Levels of form II mtDNA and SSB; ◆, HR-SEM data; ○, electrophoresis data.

[¶]The estimation from HR-SEM micrographs of the percentage of mtDNA forms is obtained from pooled micrographs and is currently the most accurate information available to us.

[‖]The factor 1.4 compensates for the increased binding of ethidium bromide to form II mtDNA (37), and is used in the estimation of SSB (38). The factor is omitted from SSB evaluated directly from HR-SEM micrographs. There was no detectable change in the amount of form III mtDNA, which therefore was omitted from calculations.

ene or probucol at 50 μM resulted in a 40.6 ± 0.4% or 42.7 ± 3.1% (n = 3) reduction in Fe(III) gluconate-caused SSB, respectively (relative to the amount of SSB without added antioxidants). Higher concentrations of antioxidants were also tried under normoxic conditions. When mitochondria were incubated in the presence 200 μM Trolox-c (6-hydroxy-2,5,7,8-tetramethylchroman-2-carboxylic acid) or butylated hydroxytoluene the Fe(III) gluconate-caused SSB were increased by 21.7 ± 7% or 1.3 ± 0.1% (n = 2), respectively. However, the addition of 200 μM of the iron chelator. Desferal resulted in 47.1 ± 0.1% (n = 2) reduction in SSB.

Iron Detection in SE and BSE Images. SE and BSE images of mtDNA samples isolated from mitochondria incubated with Fe(III) gluconate (Fig. 4 *a–f*) show metal colloids bound to DNA. Since nonmetallic, carbon-based biological samples have inherently low BSE coefficients compared with metals, the strong BSE signal appearing in areas of DNA unwinding and on strands of unwound mtDNA (Fig. 4 *b*, *d*, and *f*) unequivocally identifies the metal content of the colloid. SE and BSE images show a similar number (4 ± 2) of metal colloids bound to mtDNA with increasing iron dose. The colloids have an average size of 6.5 ± 0.7 nm (range 1–52 nm, n = 151, n is the number of colloids measured). DNA obtained from untreated mitochondria, and mtDNA treated with the metal chelator DTPA, did not contain any metal colloids (Fig. 2 *e* and inset). No metal colloids were found when mitochondria were omitted from the incubation mixture, or when the mitochondria-free incubation solution was mixed with pUC21 (Fig. 4 *g* and *h*) or pBR322 (not shown) at 300 ng/ml. Furthermore, mtDNA and pUC21 DNA mixed with reference colloids and washed by centrifugation-filtration did not show bound colloids (not shown).

DISCUSSION

HR-SEM Analysis of DNA. Conventional scanning microscopy cannot resolve nanometer-range structures, and transmission electron microscopy is unable to depict three-dimensional topography without simulated or reconstructed models. In contrast, HR-SEM imaging directly displays three-dimensional information. HR-SEM combined with BSE detection can map nanometer-range metal colloids, uniquely complementing topographic information provided by the SE (39).

DNA was prepared here in 3 mM $MgCl_2$ (29) without resorting to modifying conditions such as hypophasic spreading or the presence of ethidium bromide, cytochrome *c*, or formamide. In addition, rapid freezing used here prevents DNA width variation due to increased salt concentration (40), and it immobilizes the hydrated molecule in a physiological suspension. Hence HR-SEM micrographs show mtDNA in dimensions expected for duplex DNA—*i.e.*, the 2-nm width and 0.34-nm rise between base pairs. mtDNA visualized by HR-SEM is in the B form since the A or Z form would have measured 3749 nm or 6193 nm in length, respectively, based on the 0.34-nm rise between base pairs. Therefore, this technique permits the analysis of mtDNA in a near-native state and when it has undergone iron-induced conformational changes.

Iron Colloid Formation. Mitochondria exposed to 500 μM Fe(III) gluconate take up about 33 nmol of Fe(III) per mg of protein (P.W., unpublished result). Can the iron upon uptake bind to DNA? Double-stranded helical DNA has potential sites for metal-ion interaction at the major and minor grooves, exposing both the ribose phosphate moieties and parts of the bases; these organized centers of charge and N donors can bind heavy metal ions (41). Early experiments showed evidence that iron can bind to nucleic acids (42–46). NMR work by Eisinger *et al.* (46) suggests binding of Fe(III) and Fe(II) to the interior and exterior, respectively, of the DNA double helix. More recent experiments provide further evidence of iron–DNA adduct formation (47–49). Additionally, deposits within mitochondria of humans with sideroblastic anemia have been identified as iron phosphates (50, 51).

Our HR-SEM study, combined with BSE detection, shows that iron colloid formation takes place on mtDNA during *in vitro* iron overload of mitochondria. We believe that all iron visualized through BSE detection is associated with mtDNA since 3-fold centrifugation/filtration washing (see *Materials and Methods*) would remove all free iron and unbound colloids. Furthermore, we have ruled out nonspecific binding by finding that mtDNA and pUC21 DNA mixed with reference colloids and washed by centrifugation-filtration do not show colloids (not shown). The large size of the colloids compared with the presumed size of the Fe(III) gluconate complex suggests some form of mitochondrial processing of the iron.

In relationship to DNA damage, two DNA binding modes for iron have been suggested (52): either binding to phosphate residues or coordination in a sequence (base-) specific manner. In the latter case, iron can bind either the base and the phosphate or the base alone. We show here directly that colloidal iron indeed binds to DNA. Our experiments differ from the recently published work (52) in that we see colloidal iron bound to mtDNA, which again is probably due to mitochondrial processing of the iron. Furthermore, mitochondrial proteins may play a role in DNA binding of the iron colloids, and even constitute part of the colloid. The number of iron colloids bound to mtDNA molecules (4 ± 2) is independent of the Fe(III) dose. This suggests that the binding is base specific.

mtDNA Relaxation. Iron-induced change in overall DNA topology has previously been attributed to oxidative DNA damage caused by ·OH by the Fenton reaction (8). We find, however, that iron-induced relaxation is not completely prevented by nitrogen purging or antioxidants. We cannot exclude minute amounts of oxygen, perhaps bound to iron complexes, in mitochondria, but glucose oxidase and mitochondrial cytochrome oxidase bring the free oxygen well below 0.5 μM. Additional factors other than reactive oxygen are then apparently involved in the iron-dependent unwinding of mtDNA. For example, iron colloid growth on mtDNA could physically separate the mtDNA supercoils (see Fig. 4*c*). Colloids may prevent site-specific binding of proteins—*e.g.*, mtDNA repair enzymes and/or other mtDNA binding proteins—thereby preventing mtDNA from reforming supercoils. Possible mitochondrial reduction of Fe(III) to Fe(II) (4) followed by reaction with H_2O_2 generates ·OH or type I and II oxidants (52), which could nick the DNA strands. The resulting relaxed mtDNA molecule would be more receptive to further iron–DNA binding and iron colloid growth on DNA strands.

Conclusions. Images obtained from transmission electron microscopy techniques still provide highly useful structural information. In-lens field-emission cryo-HR-SEM, in concert with BSE detection, provides information about nanometer-level topography and heavy atom complex localization (30, 36). Molecules with highly corrugated surfaces, such as supercoiled mtDNA, are particularly suitable for this technique. HR-SEM studies can also complement structural data, from particle scatter-based modeling systems (*e.g.*, x-ray, electron diffraction) or NMR studies, by providing the *in situ* elucidation of molecular architecture. HR-SEM could thereby bridge the gap between these different methods. Although HR-SEM does not yield atomic level data, as does NMR or diffraction-based methods, HR-SEM is not limited by the size, shape, or biophysical characteristics (*e.g.* crystallizability, isotropic "tumbling") of the target molecule. Combined with the technical ease of imaging complex macromolecules, this sets the stage for a wide range of future studies—*e.g.*, the analysis of repair enzymes binding to oxidatively damaged mtDNA, metal complex and antitumor drug interactions with DNA, and immunolabeling of DNA adducts.

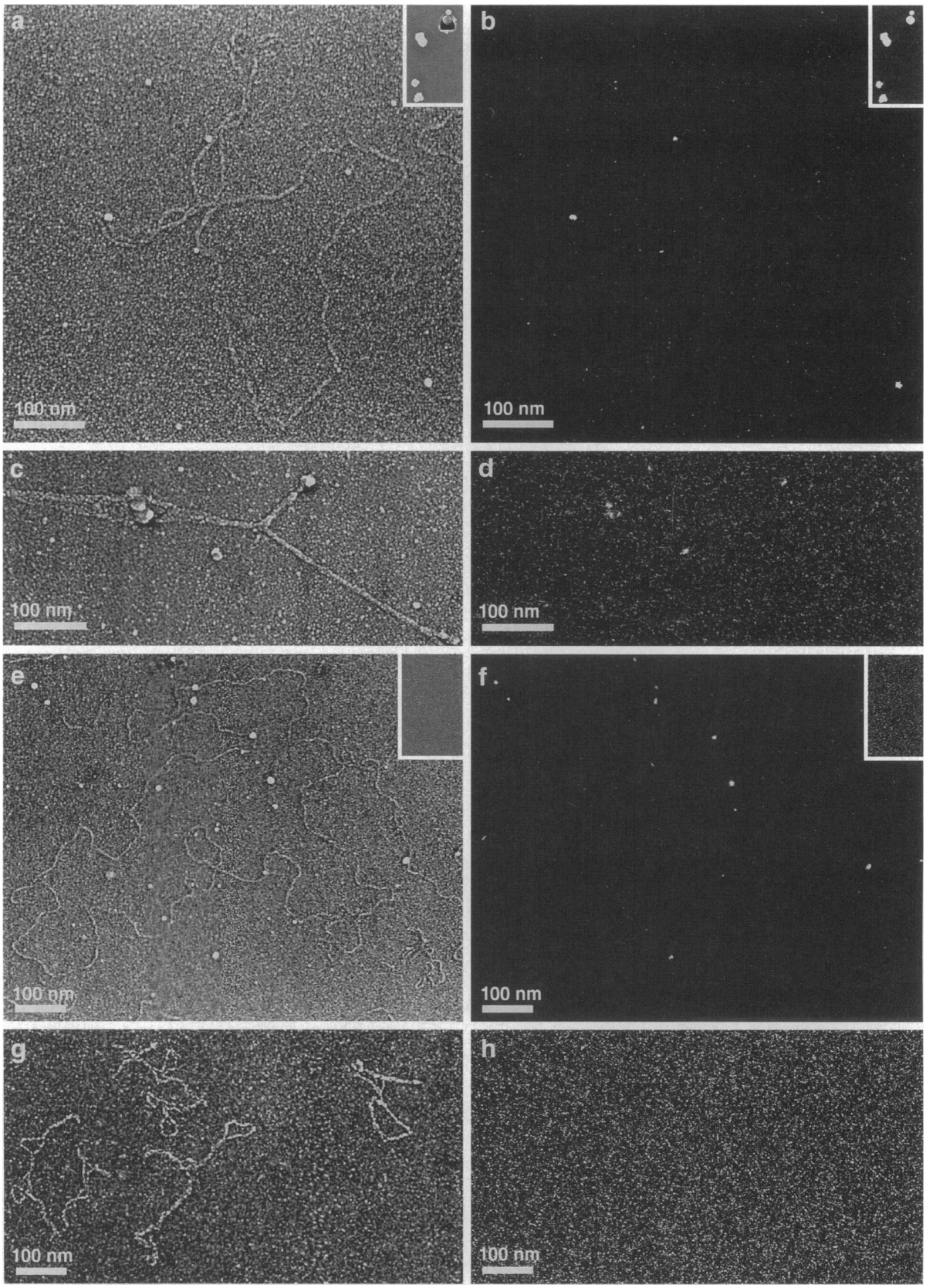

FIG. 4. Secondary and BSE detection of iron bound to mtDNA. (*a* and *c*) High magnifications of mtDNA isolated from mitochondria incubated with 250 and 500 μM Fe(III) gluconate (not treated with metal chelator DTPA). (*b* and *d*) Corresponding BSE images. (*c*) Iron colloids between two duplex strands of mtDNA. (*a* and *b insets*) Secondary and corresponding BSE images of control colloids, respectively. (*e*) Secondary electron images of mtDNA isolated from mitochondria incubated with 500 μM Fe(III) gluconate; (*f*) Corresponding BSE image. (*e* and *f insets*) Secondary and corresponding BSE images, respectively, of the incubation mixture. (*g*) pUC21 DNA mixed with Fe(III) gluconate (incubation mixture). (*h*) BSE image of *g*.

We are indebted to Willem H. Koppenol and Reinhard Kissner (Eidgenössische Technische Hochschule) for their professional input and speciation calculations, Felix Funk for providing reference iron colloids, and Alain Wasserfallen, René Hermann, and José M. Sogo for helpful suggestions and discussions. We are grateful to Marianne Suter for help with the mitochondrial experiments. We also acknowledge the pioneering work and suggestions of Margit Nass, and thank Kaspar H. Winterhalter and Hans Moor for their interest and continuing support. M.Y. and P.W. received research funds from the Swiss Federal Institute of Technology.

1. Romslo, I. & Flatmark, T. (1973) *Biochim. Biophys. Acta* **305,** 29–40.
2. Funk, F., Lecrenier, C., Lesuisse, E., Crichton, R. R. & Schneider, W. (1986) *Eur. J. Biochem.* **157,** 303–309.
3. Masini, A., Tommaso, T., Ceccarelli-Stanzani, D. & Ventura, E. (1985) *Biochim. Biophys. Acta* **810,** 20–26.
4. Flatmark, T. & Romslo, I. (1975) *J. Biol. Chem.* **250,** 6433–6438.
5. Tyler, D. (1992) *The Mitochondrion in Health and Disease* (VCH, Cambridge, U.K.), pp. 466–474.
6. Ryan, T. P. & Aust, S. A. (1992) *Crit. Rev. Toxicol.* **22,** 119–141.
7. Loschen, G., Azzi, A., Richter, C. & Flohé, L. (1974) *FEBS Lett.* **42,** 68–72.
8. Dizdaroglu, M. (1993) in *DNA and Free Radicals,* eds. Halliwell, B. & Aruoma, O. (Ellis Horwood, Chichester, U.K.), pp. 19–39.
9. Singh, G., Hauswirth, W., Ross, W. & Neims, A. H. (1985) *Mol. Pharmacol.* **27,** 167–170.
10. Lim, L. O. & Neims, A. H. (1987) *Biochem. Pharmacol.* **36,** 2769–2774.
11. Hruszkewycz, A. M. (1988) *Biochem. Biophys. Res. Commun.* **153,** 191–197.
12. Itoh, H., Shioda, T., Matsura, T., Koyama, S., Nakanishi, T., Kajiyama, G. & Kawasaki, T. (1994) *Arch. Biochem. Biophys.* **313,** 120–125.
13. Higuchi, Y. & Linn, S. (1995) *J. Biol. Chem.* **270,** 7950–7956.
14. Fairfield, F. R., Bauer, W. R. & Simpson, M. V. (1979) *J. Biol. Chem.* **254,** 9352–9354.
15. Kosovsky, M. J. & Soslau, G. (1993) *Biochim. Biophys. Acta* **1164,** 101–107.
16. Gadaleta, M. N., Pepe, G., DeCandia, G., Quagliariello, C., Sbisa, E. & Saccone, C. (1989) *J. Mol. Evol.* **28,** 497–516.
17. Richter, C. (1995) in *Molecular Aspects of Ageing,* Dahlem Konferenz 74, eds. Esser, K., & Martin, G. M. (Wiley, New York), pp. 99–108.
18. Shigenaga, M. K., Hagen, T. M. & Ames, B. N. (1994) *Proc. Natl. Acad. Sci. USA* **91,** 10771–10775.
19. Richter, C., Park, J.-W. & Ames, B. N. (1988) *Proc. Natl. Acad. Sci. USA* **85,** 6465–6467.
20. Wallace, D. C. (1992) *Science* **256,** 628–632.
21. Lewis, J. R. (1993) *Hawley's Condensed Chemical Dictionary* (Van Nostrand Reinhold, New York), 12th Ed., pp. 300–301.
22. Hibbert, D. B. & James, A. M. (1987) *Macmillan Dictionary of Chemistry* (Macmillan, London), pp. 111–112.
23. Klingenberg, M. & Slenczka, W. (1959) *Biochem. Z.* **331,** 486–517.
24. Pecsok, R. L. & Sandera, J. (1955) *J. Am. Chem. Soc.* **77,** 1489–1494.
25. Shepherd, R. E., Isaacson, Y., Chensny, L., Zhang, S., Kortes, R. & John, K. (1993) *J. Inorg. Biochem.* **49,** 23–48.
26. Martell, A. E. & Motekaitis, R. (1993) *Critical Stability Constants,* Data Base Number 46 (National Institute of Standards, Gaithersburg, MD).
27. Frei, B., Winterhalter, K. H. & Richter, C. (1985) *J. Biol. Chem.* **260,** 7394–7401.
28. Gibson, Q. H., Swoboda, B. E. P. & Massey, V. (1964) *J. Biol. Chem.* **239,** 3927–3931.
29. Sogo, J., Stasiak, A., De Bernardin, W., Losa, R. & Koller, T. (1987) in *Electron Microscopy in Molecular Biology: A Practical Approach,* eds. Sommerville, J. & Scheer, U. (IRL, Oxford), pp. 61–78.
30. Hermann, R., Pawley, J., Nagatani, T. & Müller, M. (1988) *Scanning Microsc.* **2,** 1215–1230.
31. Autrata, R., Hermann, R. & Müller, M. (1992) *Scanning* **14,** 127–135.
32. Watson, N. (1988) *Gene* **70,** 399–403.
33. Vieira, J. & Messing, J. (1991) *Gene* **100,** 189–194.
34. Astbury, W. T. & Bell, F. O. (1938) *Nature (London)* **141,** 747–748.
35. Adams, R. L. P., Knowle, J. T. & Leader, D. P. (1992) *The Biochemistry of Nucleic Acids* (Chapman and Hall, London), 11th Ed., pp. 14–19.
36. Hermann, R. & Müller, M. (1991) *Scanning Microsc.* **5,** 653–664.
37. Lloyd, R. S., Haidle, C. W. & Robberson, D. L. (1978) *Biochemistry* **17,** 1890–1896.
38. Epe, B., Mützel, P. & Adam, W. (1988) *Chem.-Biol. Interact.* **67,** 149–165.
39. Hermann, R., Schwarz, H. & Müller, M. (1991) *J. Struct. Biol.* **107,** 38–47.
40. Bednar, J., Furrer, P., Stasiak, A., Dubochet, J., Egelman, E. H. & Bates, A. D. (1994) *J. Mol. Biol.* **235,** 825–847.
41. Fraústo Da Silva, J. J. R. & Williams, R. J. P. (1991) *The Biological Chemistry of the Elements: The Inorganic Chemistry of Life* (Clarendon, Oxford), pp. 188–219.
42. Wacker, W. E. C., Gordon, M. P. & Huff, J. W. (1963) *Biochemistry* **2,** 716–719.
43. Wacker, W. E. C. & Vallee, B. L. (1959) *J. Biol. Chem.* **234,** 3257–3262.
44. Haschemeyer, R., Singer, B. & Fraenkel-Conrat, H. (1959) *Proc. Natl. Acad. Sci. USA* **45,** 313–319.
45. Loring, H. S. & Waritz, R. S. (1957) *Science* **125,** 646–648.
46. Eisinger, J., Shulman, R. G. & Blumberg, W. E. (1961) *Nature (London)* **192,** 963–964.
47. Shires, T. K. (1982) *Biochem. J.* **205,** 321–329.
48. Richardson, C. L., Verna, J., Schulman, G. E., Shipp, K. & Grant, A. D. (1981) *Environ. Mutagen.* **3,** 545–553.
49. Sakurai, K., Haga, K. & Ogiso, T. (1994) *Biol. Pharm. Bull.* **17,** 227–231.
50. Trump, B. F., Berezesky, I. K., Jiji, R. M., Mergner, W. J. & Bulger, R. E. (1978) *Lab. Invest.* **39,** 375–380.
51. Grasso, J. A., Myers, T. J., Hines, J. D. & Sullivan, A. L (1980) *Br. J. Haematol.* **46,** 57–72.
52. Luo, Y., Han, Z., Chin, S. M. & Linn, S. (1994) *Proc. Natl. Acad. Sci. USA* **91,** 12438–12442